CARPATHIAN JOURNAL OF FOOD SCIENCE AND TECHNOLOGY

journal homepage: **http://chimie-biologie.ubm.ro/carpathian_journal/index.html**

OPEN ACCESS

CC BY SA

Research article

PROTEOMIC INSIGHTS INTO THE MECHANISM OF ENHANCING EGG WHITE FUNCTIONALITY WITH SNAKEHEAD FISH SKIN COLLAGEN PEPTIDES

Ruihan Yu[1], Yingjian Wang[2], Shirong Dong[1], Chun Bian[1]✉, Yanfeng Qu[1]

[1]College of Food Engineering, Harbin University, Harbin 150000, China
[2]School of Chemistry and Molecular Bioscience, Queensland University, Brisbane, Queensland, Australia, 4072
✉Corresponding author: Chun Bian Email: bianchun1980@126.com, Tel.: 0451-86655794 (C.B.); quyanfeng01@sina.com, Tel.: 0451-86621936 (Y.Q.)

https://doi.org/10.34302/crpjfst/LKHK6463

Article history:
Received:
December 6th 2025
Accepted:
July 21th 2026
Published:
November 23th 2026

Keywords
Snakehead fish skin collagen; Peptide (SFSCP); Egg white; Nutritional value; Functional and physicochemical properties.

Abstract
This study analyzed the amino acid sequence of collagen peptides derived from snakehead fish skin collagen peptide (SFSCP). Through LC-MS/MS peptide identification, 1,835 distinct peptide segments were obtained from the enzymatic hydrolysis of SFSCP, and these peptides were matched to 144 proteins by using the uniprotkb database. The sequences of SFSCP were matched functional protein of beneficial to human health, such as myosin regulatory light chain 2, apolipoproteins, and lumican. In this study, 0%, 1%, 2%, 3% and 4% SFSCP were added to egg white (EW) liquid, respectively. The results showed that with the contents of SFSCP increasing, the particle size, sulfhydryl group, the foaming properties, the gel properties, a-helix and b-sheets was increased, however, the surface hydrophobicity was decreased. This study showed that the addition of SFSCP to EW might enhance the nutritional value of EW and increase functional properties.

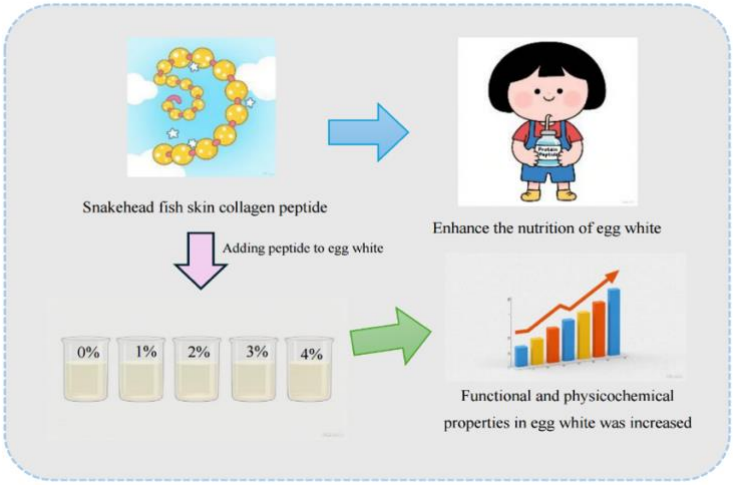

Graphical abstract

1. Introduction

Heilongjiang Province is a major production area for snakehead fish(M. Li et al., 2025). The snakehead fish meat with tender and nutritious, which could be suitable for various cooking methods. Snakehead fish with few bones was suitable for the elderly and children (Rahman et al., 2025). The slime on the fish skin is primarily composed of trimethylamine and aminopentanal compounds, which contribute to the fishy odor (Thinthasit, Nugroho, Petsong, Surya, & Benchawattananon, 2025). As previous results showed, fish skin was often discarded during food production. Aquatic collagen avoids potential risks such as foot-and-mouth disease and mad cow disease. Additionally, it is low in fat, making it highly favored by those on weight-loss diets (Michael et al., 2024)**.**

In previous research indicated that orally administered collagen peptides could be absorbed as free amino acids in humans, meanwhile, certain oligopeptides could also be directly absorbed through the intestinal epithelium via the PepT1-mediated transport system (Chi et al., 2024). Consequently, incorporating collagen peptides derived from snakehead fish skin collagen peptide (SFSCP) into food products could significantly enhance their nutritional profile (J. Zhang et al., 2021). Through enzymatic hydrolysis and sequencing of SFSCP, followed by matching with protein databases, it was found that the sequences of collagen peptides from SFSCP partially align with functional proteins such as calcium-transporting ATPases, apolipoproteins and lumican.

These results suggested that dietary supplementation with collagen peptides derived from SFSCP might enhance calcium absorption, immune function and support visual health. The current study provides both theoretical foundations and technical references for the comprehensive utilization of by-products from snakehead fish processing and production, demonstrating significant practical value for industrial applications.

China is currently a major egg producing country, ranking first place globally in egg production (X. Liu et al., 2025). Egg white (EW) with low contents of fat and high absorbability by the human body, which are an ideal source of healthy protein (L. Liu et al., 2025). Additionally, EW had foaming and gel properties, therefore, EW was an important raw material in the food industry (Lihui Zhang, Zang, Gao, Chen, & Tong, 2025).

In this study, SFSCP were added to EW with concentrations of 0%, 1%, 2%, 3%, and 4%, respectively. This study showed that with the concentration of SFSCP in EW were increased, the foaming and gelling properties of the EW increasing. In previous studies, improving the gelation and foaming properties of EW was typically achieved by adding sucrose or NaCl (Yan, Han, Xue, Wang, Tu, & Zhao, 2025). However, excessive consumption of sucrose or NaCl might increase the risk of chronic diseases such as hypertension and hyperlipidemia (Omotosho et al., 2025). This research showed that adding SFSCP to EW liquid could enhance nutritional value of EW, meanwhile, EW liquid functional properties could also be increased with the SFSCP concentration increasing. SFSCP was cost-effective and readily available.

Further analysis revealed that when the contents of SFSCP in EW liquid was increased, the contents of α-helix, β-sheet, sulfhydryl group, disulfide bond and particle size in EW increasing, however, surface hydrophobicity decreasing. Therefore, these results indicated that the change of EW liquid physicochemical verified the alteration of the EW liquid functional properties. This research provided a theoretical foundation and direction for the development of animal-derived protein products, thus enriching the variety of EW-based food products.

2. Materials and methods

2.1. Samples and reagents

Fresh snakehead fish and eggs were obtained from a local supermarket in Harbin County, Heilongjiang Province, China. Reagents 5,5′-dithiobis-(2-nitrobenzoic acid) (DTNB) Pepsin (700 U/g), Trypsin (1500 U/mg) and β-mercaptoethanol were purchased from

Sigma-Aldrich (St. Louis, MO, USA). Acetonitrile, and trifluoroacetic acid, Isopropanol, sodium hydroxide, concentrated sulfuric acid, concentrated hydrochloric acid, boric acid, potassium persulfate, dimethyl sulfoxide: were obtained from Solarbio Science & Technology Co., Ltd. (Beijing, China). The acetonitrile, trifluoroacetic acid, and water used in the HPLC analysis were HPLC grade. All other chemicals used in the study were analytical grade.

2.2. Pretreatment of Snakehead Fish Skin

The snakehead fish skin (SFS) was rinsed thoroughly under running water. Then, the SFS was immersed by 0.1 mol/L NaOH solution at a ratio of 1:30 (w/v), with the solution replaced every 12 h, and soaked at 4°C for 1 d (Kim et al., 2025). After NaOH treatment, the SS was washed three times with deionized water until neutral. Subsequently, the SS was degreased with 10% (w/v) isopropanol at a ratio of 1:30 (w/v), soaked at 4 °C for 1 d with the solution replaced every 12 h, and finally rinsed with deionized water until neutral (Xu et al., 2025).

2.3. Enzymatic extraction of snakehead fish skin collagen

The SFS was mixed with a 0.5 mol/L acetic acid solution with ratio of 1:20 (w/v). A predetermined amount of pepsin was added to the acetic acid solution, and enzymatic hydrolysis was carried out at 4 °C for 24 h. After hydrolysis, the enzyme was inactivated by heating at 80 °C for 10 min. The hydrolysate was filtered through gauze, and the filtrate was centrifuged at 9000 × g for 20 mins to collect the supernatant. NaCl was added to the crude extract to achieve a final NaCl concentration of 0.9 mol/L. The mixture was then subjected to NaCl precipitation overnight at 4°C, then centrifugated by 9000 × g (Ma et al., 2023). Then, the supernatant was discarded, and the precipitate was dissolved in 0.5 mol/L acetic acid solution. The crude collagen solution was transferred into a dialysis bag and dialyzed first against 0.1 mol/L acetic acid for 1 d, and then deionized water for 2 d. The dialysis buffer was replaced at least three times daily. Final, the dialyzed sample was freeze-dried under vacuum to obtain SS peptide powder (Munawaroh et al., 2023).

2.4, Chromatographic analysis of peptide

The mobile phases consisted of Solvent A (0.1% formic acid in water) and Solvent B (0.1% formic acid in acetonitrile/water, 84% acetonitrile), with the liquid chromatography analytical column (0.15 mm × 150 mm, RP-C18, Column Technology Inc.) (Li, Chang, Qiu, Yang, Xue, & Zheng, 2025). The samples were equilibrated with 95% Solvent A prior before analysis. Samples were automatically loaded onto Zorbax 300SB-C18 peptide traps (Agilent Technologies, Wilmington, DE) and subsequently separated on the analytical column using a gradient program that initiated with a linear was increased of Solvent B from 4% to 50% over 50 mins, and then a steeper gradient from 50% to 100% between 50 and 54 mins, and maintained at 100% Solvent B from 54 to 60 mins to complete the elution (Wagner et al., 2025).

2.5. Peptide mass spectrometry identification

The enzymatically digested peptides were separated by capillary high-performance liquid chromatography and subsequently analyzed using Q Exactive HF-X mass spectrometer (Thermo Fisher) over a 60 mins acquisition period in positive ion mode. Mass-to-charge ratios of both parent peptides and their fragments were acquired through a data-dependent acquisition method, where each full scan (MS1) was followed by 10 tandem mass spectra (MS2). The raw mass spectrometry data files were processed using MaxQuant software (version 1.5.5.1) with the following search parameters: enzyme specification: none; maximum allowed missed cleavages: 2; fixed or variable modifications applied: none; reference database: uniprotkb; reverse decoy database pattern for false discovery rate (FDR) estimation; precursor ions mass tolerances: 20 ppm and 0.1 Da for fragment ions; protein-level threshold≤0.01 (Luo, Xu, & Ji, 2025).

2.6. Pretreatment protein sample

The fresh eggs were washed and shelled, and the egg whites（EW）were stirred at 220 r/min for 30 min using a magnetic stirrer and then filtered through double-layered gauze to obtain the experimental samples (S. Li et al., 2025). Snakehead fish skin collagen peptide (SFSCP) was added to the EW with concentrations of 0%, 1%, 2%, 3%, and 4%, respectively. The mixtures were stirred at 240 r/min for 20 mins with a magnetic stirrer to ensure complete dissolution of the peptides, obtaining the final test samples for this study. Three replicate samples were measured for each treatment.

2.7. The foam property

Boric Acid-Sodium Hydroxide Buffer Solution: Buffer solution was prepared by dissolving 9 g of boric acid and 3.6 g of sodium hydroxide in distilled water, which was then diluted to a final volume of 1000 mL. The EW liquid was stirred for 30 mins using a magnetic stirrer and subsequently filtered through gauze. The filtrate was diluted 10 times with the boric acid-sodium hydroxide buffer solution. The mixture was homogenized at 12,000 r/min for 1 min to determine foaming capacity. After standing for 30 min, the total volume of foam and liquid was measured (Ding et al., 2025). The foaming capacity was calculated by Foaming capacity = (Va - Vb) / Vb, where Va is the Total volume of foam and liquid; Vb is the Initial liquid volume. The foam stability was calculated by Foam stability = Vc / Vd, where Vc is the Bubble volume after 30 min; Vd is the Initial foam volume.

2.8. The gel property

The samples were heated under 90 °C water bath for 20 min. The heated samples were immediately cooled under running water and then stored at 4 °C for 24 h to analyze. The samples were allowed to equilibrate to room temperature before testing. Texture profile analysis was conducted at 25 °C using a texture analyzer with the following parameters: pre-test speed of 5.0 mm/s, test speed of 2.0 mm/s, post-test speed of 2.0 mm/s, compression distance of 10 mm, and trigger force of 5 g (T. Zhang, Gong, Zhang, Xu, Liu, & Shang, 2025).

2.9. Contents of sulfhydryl group

For surface sulfhydryl group analysis, 1 g samples were dissolved in 100 mL buffer 1 (0.086 mmol/L Tris, 0.19 mmol/L Glycine, 4 mmol/L EDTA, and 8 mol/L urea), vortexed for 3 min, and then reacted with 0.1 mL of EUman reagent in the dark at room temperature for 20 min. After centrifugation at 5000 × g for 15 min, the supernatant was collected, and its absorbance was measured at 412 nm.

For total sulfhydryl group analysis: 1 g of the sample was dissolved in 100 mL of Buffer 2 (0.086 mmol/L Tris, 0.19 mmol/L Glycine, 4 mmol/L EDTA, 8 mol/L urea, 10 mmol/L β-mercaptoethanol). The mixture was vortexed for 3 mins, followed by the addition of 0.1 mL of Ellman's reagent. The reaction was kept in the dark at room temperature for 20 mins. The solution was then centrifuged at 5000 × g for 15 mins, and the supernatant was collected. The absorbance of the sample was measured at 412 nm (Margaritis et al., 2011).

The contents of disulfide bond in EW samples were calculated by Disulfide bond (SS) = (SHt - SHs) / 2, where SHt is the content of Total sulfhydryl groups; SHs is the contents of Surface sulfhydryl groups (Husted, Sørensen, & Sottrup-Jensen, 2003).

2.10. Surface hydrophobicity

The surface hydrophobicity of different samples was investigated using the ANS (1-anilinonaphthalene-8-sulfonate) fluorescence probe method. Approximately 0.5 g of each EW sample was dissolved in 0.01 mol/L phosphate buffer (pH 7.0), followed by centrifugation at 4,000 × g for 10 mins. The supernatant was filtered through a 0.22 mm microporous membrane. The soluble protein content was determined by the Lowry method, and the samples were subsequently diluted with the same buffer. For fluorescence measurement, 5 mL of the protein sample was mixed with 25 mL of ANS probe solution (8 mmol/L in 0.01 mol/L phosphate buffer, pH 7.0) and incubated at room temperature for 15 mins. The fluorescence

intensity (FI) of the sample was measured both before and after ANS addition. The surface hydrophobicity index was calculated as the slope of the curve obtained by plotting FI against protein concentration. All measurements were performed in triplicate under controlled conditions (25 °C, dark environment) using a fluorescence spectrophotometer with excitation at 390 nm and emission at 470 nm (Lin et al., 2025).

2.11. analysis of particle size

Each sample was diluted 10 times with ultrapure water and vortex-mixed for 10 s to ensure complete dissolution. Following centrifugation at 5,000 × for 15 mins, the supernatant was collected for particle size analysis. Measurements were conducted using a MICROTRAC S3500 laser diffraction particle size analyzer to determine D[4.3] (volume mean diameter), D10, D50, D90, and the volumetric particle size distribution profile (Balis, Gochev, Truzzolillo, Lupa, Szyk-Warszynska, & Zawala, 2025).

2.12. Protein secondary structure

The liquid sample was uniformly deposited on a microscope slide for Raman spectroscopy measurements. Spectral acquisition was performed under the following parameters: spectral range of 400-2000 cm-1, 532 nm excitation wavelength, 50 mW laser power, with peak position accuracy maintained within ±3 cm-1. The phenylalanine band at (1003±1) cm-1 was used as the internal reference for spectral normalization. Raw spectra were processed using OMNIC software for baseline correction and peak assignment. Subsequent quantitative analysis of protein secondary structure was conducted through deconvolution of the amide I band (1600-1700 cm-1) using PeakFit 4.12 software (Systat Software Inc.) (Banthia, McKenna, Tiwari, & Dubey, 2025). With Gaussian-Lorentzian curve fitting to determine the relative percentages of a-helix, b-sheet, b-turn and random coil conformations.

2.13. Data analysis

SPSS 27.0 was used in this research, all results were tested in three times. Data in the table are expressed as the means ± standard deviation with variance analysis (ANOVA) and Duncan's multiple-range test ($p < 0.05$) processed. Figures were plotted by OriginPro 2024 (OriginLab Co., MA, USA).

3. Results and discussions

3.1 Total ion flow chromatography

The total ion current (TIC) chromatogram of SFSCP was shown in Fig. 1. The chromatographically separated peptide components were introduced into the mass spectrometer for continuous scanning, generating an ion chromatogram with ion intensity as the y-axis and retention time as the x-axis. The TIC was obtained by summing the intensities of all ions in each mass spectrum. Each peak in the TIC represents a distinct compound, where the distance between adjacent peaks indicates their separation degree (Herman, Xu, Traylor, Ghose, Li, & Lenhoff, 2022). Higher resolution values reflect greater differences in chromatographic retention times between components, demonstrating better separation performance (Kobelt, Lippmann, Wuttke, Wessel, & Zimmermann, 2024). Different peptide fragments eluted at distinct retention times, achieving effective separation. The SFSCP study showed good overall separation, as evidenced by well-resolved peaks in the chromatogram. This successful separation establishes a solid foundation for subsequent peptide sequencing analysis.

3.2. Analysis of peptide sequencing results

The snakehead fish skin was enzymatically digested to obtain 1,835 different peptides, which were matched to 144 proteins using the UniProtKB database. Due to the large number of proteins, it was difficult to display all of them. Therefore, this study selected and presented the sequencing results of protein peptides related to human immunity, sports rehabilitation, and nutritional health. Partial results and matching outcomes are shown in Table 1. The first column lists the peptide sequences, the second column

shows the peptide length, the third column displays the protein names, and the fourth column describes the protein functions. As shown in table 1, SFSCP were demonstrated to possess substantial nutritional value. The incorporation of SFSCP into EW was found to significantly enhance the nutritional profile of EW-based products. This study provided a theoretical foundation for further research and utilization of SFSCP bioactive components. This study provided a theoretical basis for further research on snakehead fish. Proteomics was characterized by high-throughput capacity, high resolution, and strong reproducibility (Kuo et al., 2025). Through proteomic approaches, protein molecules were simultaneously identified and quantified in parallel analyses, representing cutting-edge research that was demonstrated to have significant guiding value for practical production applications (Bhavsar, Kalita, Taunk, & Rapole, 2025). Moreover, proteomics was successfully employed to systematically investigate the protein composition of SFSCP, representing a significant advancement in food science theory (Lou, Lim, Li, Yu, & Gunaratne, 2025).

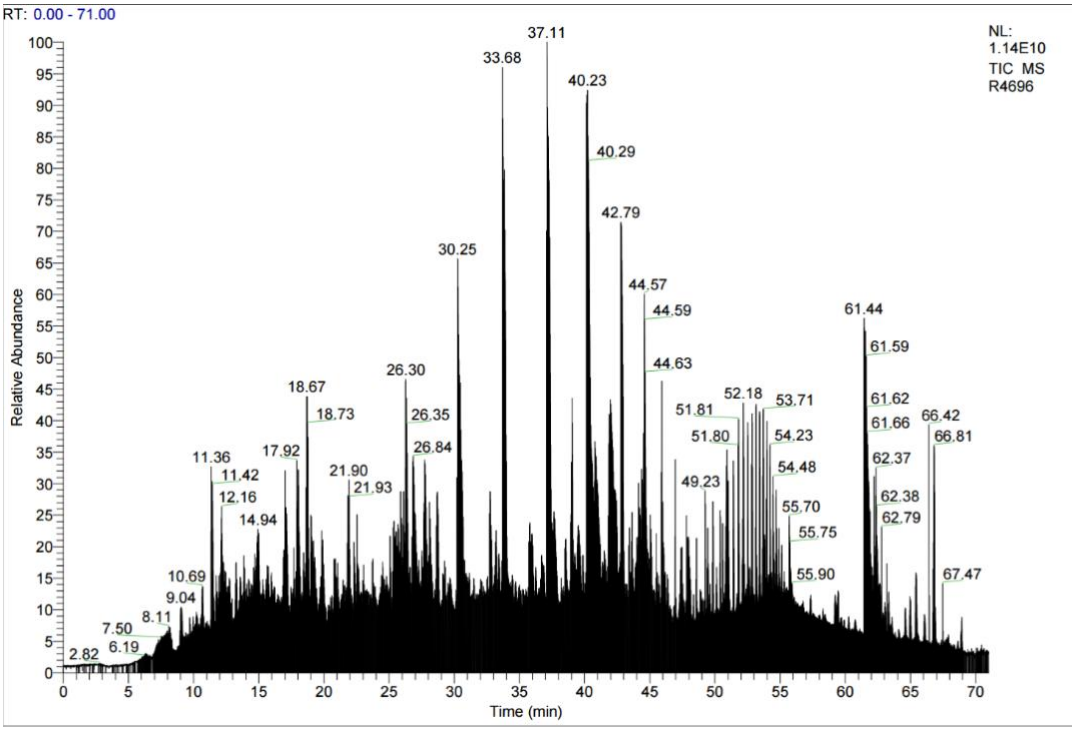

Figure 1. Total ion current chromatogram of SFSCP.

Table 1. Identifying functional proteins through SFSCP matching.

Peptide segment length	Protein names	Protein fuction
9	Collagen alpha-1(I) chain Alpha-1 type I collagen	Maintains tissue structural integrity and strength
18	Caveolae-associated protein 1	Inhibits cancer cell proliferation
11	Ig mu chain C region secreted form	Has broad antigen-binding capacity and immunomodulatory functions
19	Intermediate filament protein ON3	Involved in the regulation of cytoskeletal system functions

11	Pyruvate kinase (EC 2.7.1.40)	Provides energy for cells and maintains glucose metabolism balance
11	Calcium-transporting ATPase (EC 7.2.2.10)	Maintains cellular calcium ion concentration
13	Myosin heavy chain, fast skeletal muscle	Directly participates in the conversion of chemical energy into mechanical force
13	Periostin	Tendon formation and repair
13	Protein S100-A14 S100 calcium-binding protein A14	Binds to calcium ions
10	Annexin	Cell membrane repair and clearance of apoptotic cells
14	Major vault protein	Inhibits viral replication
13	Troponin T, fast skeletal muscle isoform	Plays a key regulatory role in muscle contraction and relaxation
19	creatine kinase (EC 2.7.3.2)	Involved in energy metabolism
12	Calcium-transporting ATPase (EC 7.2.2.10)	Catalyzes ATP hydrolysis on the inner side of the plasma membrane, releasing energy
13	PDZ and LIM domain protein 7	Inhibits obesity
22	Desmin	Ensures energy supply and calcium ion release
12	Histone H2B 1/2	Involved in DNA replication
15	AMP deaminase (EC 3.5.4.6)	Participates in purine metabolism and immunity
9	Apolipoprotein A-II	Hydrolyzes triglycerides in chylomicrons and very low-density lipoproteins
12	Keratin, type I cytoskeletal 19 Cytokeratin-19	An important biomarker for non-small cell lung cancer
22	Glyceraldehyde-3-phosphate dehydrogenase (EC 1.2.1.12)	Key protein involved in glucose metabolism
15	creatine kinase (EC 2.7.3.2)	Generates ATP
15	Neuroblast differentiation-associated protein AHNAK Desmoyokin	Promotes neuronal cell development
12	Elongation factor 1-alpha	Promotes polypeptide chain elongation during mRNA translation
15	Lumican	Maintains corneal transparency
10	Nebulin	Stabilizes and regulates actin structure
11	Myosin regulatory light chain 2, skeletal muscle isoform type 2	Anti-cancer

3.3. Function properties

3.3.1. Foaming properties

The foaming properties of EW liquid with different contents levels of SFSCP was shown in Fig. 2 (A). When the contents of SFSCP was 0%, the foaming capacity and foam stability of the sample were 29.17% and 60.27%, respectively. As the contents of SFSCP in samples were increased, the foaming capacity and foam stability of EW liquid increased. When the contents of SFSCP in samples were 4%, the foaming capacity and foam stability of the

sample were 51.02% and 86.83%, respectively. The foaming properties of proteins were widely utilized in the food industry such as cakes, marshmallows, ice cream, beer, and bread (Xiao et al., 2025). The stability of foam was formed by proteins, water, and air under specific conditions, which was determined by the interactions between protein molecules (X. Li et al., 2025). Previous research showed that the adsorption of proteins at the air-water interface played a critical role in the formation and stability of food dispersion systems, such as foam (Qing, Zang, Liu, Chi, & Chi, 2025). Therefore, the contents of SFSCP could be improved nutritional value of EW liquid and might be enhanced the foaming properties of EW products.

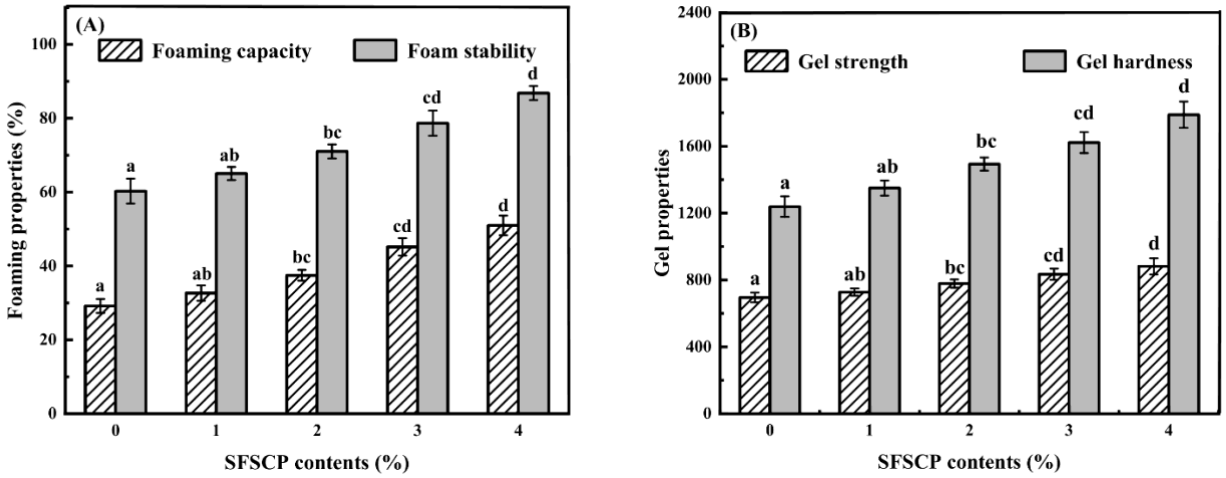

Figure 2. The functional characteristics of the samples. (A) The foaming properties of the samples. (B) The gel properties of the samples. Three replicate samples were measured for each treatment

3.3.2. Gel properties

The gel strength and gel hardness of heat-induced gels from EW liquid with different concentrations of SFSCP were shown in Fig. 2 (B). When the SFSCP content was 0%, the gel strength and gel hardness of the sample was 695.19 g and 1238.87 g, respectively. With the contents of SFSCP increased, both the gel strength and hardness of the EW liquid increased. When the SFSCP content was 4%, the gel strength and gel hardness was 881.60 g and 1788.52 g, respectively. Heat gel are inherently elastic and have numerous applications in food products (D. Yu et al., 2025). In this study, SFSCP were added to EW, where the results might be interacted with EW proteins to form a three-dimensional network structure, enhancing the gel properties of the food. As shown in table 1, the contents of disulfide bond in the samples were increased with the contents of SFSCP increasing. These results confirmed that the gel strength and gel hardness were positively correlated with the contents of disulfide bond in the samples (Tseng, Yang, Chen, Chen, Shiu, & Wang, 2025). This research demonstrated that adding SFSCP to EW could enhance the gel strength and gel hardness of EW products.

3.4 Physicochemical properties

3.4.1. Analysis of surface hydrophobicity

The changes in surface hydrophobicity of the samples with different concentrations of SFSCP was shown on Fig. 3 (A). With the content of SFSCP increased, the surface hydrophobicity in sample was decreasing. The sample with 4% SFSCP had the highest surface hydrophobicity (162.64), while the sample with 0% SFSCP was the lowest (267.78). The surface hydrophobicity was defined as the resistance to wetting exhibited by a material's surface, where interactions between the surface and water or other polar substances were significantly hindered, resulting in markedly reduced water adhesion (Ming, Xu, Chang, Zhang, Wang, &

Zhang, 2025). Hydrophobic interactions were defined as intermolecular forces generated by polarity differences between substances (Du et al., 2024). When particles possessed relatively regular shapes and low surface roughness, hydrophobic particles were generally observed to aggregate through these hydrophobic interactions (De la Cruz-Torres et al., 2022). The results demonstrated that with the contents of SFSCP in the samples was increased, the samples exhibited enhanced hydrophilicity and greater stability, meanwhile, the surface hydrophobicity was decreased. As shown in Fig. 2 and Fig. 3, with the contents of SFSCP increased, the foaming and gel properties of the EW liquid were increased, while surface hydrophobicity in samples were decreased. This result indicated that low surface hydrophobicity could enhance the functional properties of the sample.

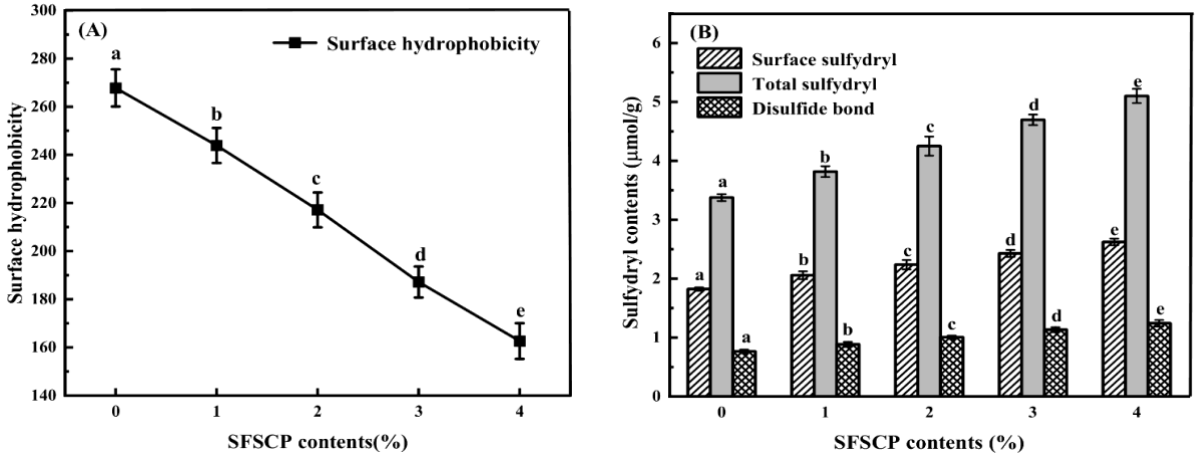

Figure 3. (A) The Surface hydrophobicity of the samples. (B) The contents of Sulfhydryl group in different samples. Three replicate samples were measured for each treatment.

3.4.2. Analysis of sulfhydryl group

Fig.3 (B) showed the content of sulfhydryl group in EW samples with different contents of SFSCP. When SFSCP content in the EW was 0%, the surface sulfhydryl groups (1.82 mmol/g), total sulfhydryl groups (3.38 mmol/g), and disulfide bonds (0.78 mmol/g) in the samples were the lowest, respectively. As the content of SFSCP was increased, the contents of surface sulfhydryl groups, total sulfhydryl groups, and disulfide bonds in the samples increased, meanwhile, when SFSCP content in the EW was 4%, the surface sulfhydryl groups (2.62 mmol/g), total sulfhydryl groups (5.10 mmol/g), and disulfide bonds (1.24 mmol/g) in the samples were the highest, respectively. A sulfhydryl group was consisted of a sulfur atom and a hydrogen atom, and disulfide bonds could interconvert with sulfhydryl groups (Yang, Li, Zhang, Wang, & Liu, 2025). The disulfide bonds could enhance protein-protein interactions, which occurred during heat protein gelation (M. Zhang et al., 2025). Additionally, protein denaturation promoted intermolecular covalent and non-covalent interactions, including disulfide bonds and hydrophobic interactions. Therefore, gel strength and gel hardness were depended on the extent of disulfide bond formation, leading to a stable network that enhanced gel strength. The disulfide bond content was positively correlated with the gel strength and hardness of the protein samples.

As shown in Fig. 2 (B), gel strength and gel hardness of the samples were increased with the concentration of SFSCP increasing. These results confirmed that the gel strength and gel hardness increased along with the disulfide bond content. The heat-induced gels prepared from egg white solution with added SFSCP exhibited excellent gel strength and hardness, therefore, these results suggested that the SFSCP EW might be suitable for industrial-scale production.

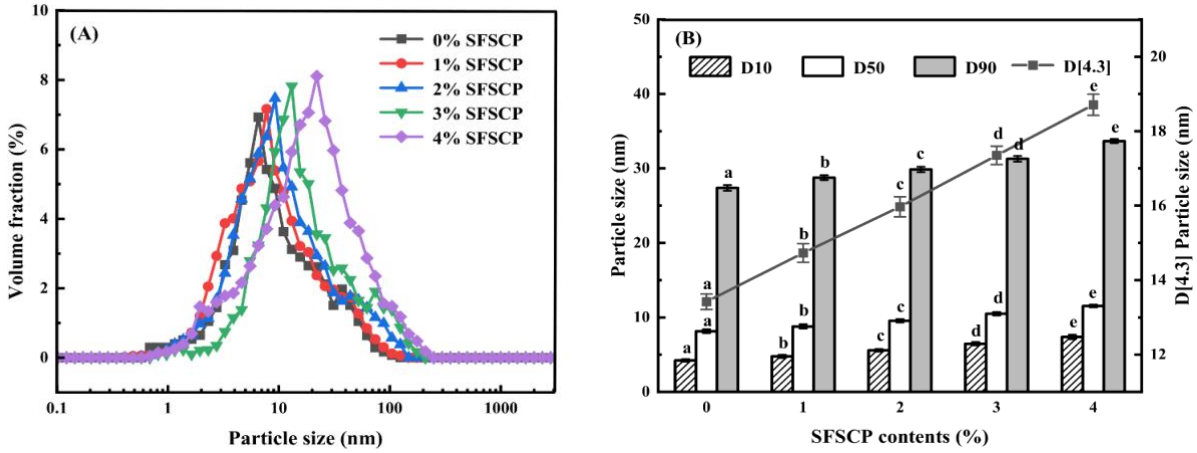

Figure.4. The particle size of the samples. (A) The particle size distribution curve. (B) The particle size of the samples. Three replicate samples were measured for each treatment.

3.5. Particle size

The particle size distribution curve was shown on Fig. 4 (A), and the particle size under different contents of SFSCP was shown in Fig. 4 (B). Particle size was found to significantly influence the texture and processing properties of food products (Ali, Parhi, & Sharma, 2025). The precise control of particle size was demonstrated to be crucial for optimizing food quality during product development (Geiss et al., 2025). Specific functional properties were associated with smaller particles, whereas improved gelation capacity was typically exhibited by larger particles (Lulu Zhang, Qiao, Liu, Wang, & Ma, 2024). The particle size distribution curve was constructed by plotting particle size along the x-axis against percentage content on the y-axis, with each data point being connected to form the particle size curve. As shown in Fig. 4 (A), the samples containing 4% SFSCP were found to display the rightmost position on the curve, indicating the presence of larger particle sizes. In contrast, albumin samples with 0% SFSCP content were observed to occupy the leftmost position on the distribution curve, confirming that these samples contained the smallest particle sizes among this study.The particle size of spherical particles was expressed by the diameter. For irregularly shaped particles in food, the diameter of a sphere exhibiting equivalent behavior could be considered as the equivalent diameter of the particle (Yao, Williams, Mikkelsen, Flanagan, & Gidley, 2023). Particle size was typically shown by D[4.3], D10, D50 and D90, where D[4.3] represented the mean particle diameter of the sample, D10 denoted the particle size at 10% cumulative distribution, D50 indicated the median particle size at 50% cumulative distribution, and D90 corresponded to the particle size at 90% cumulative distribution (Yao, Flanagan, Williams, Mikkelsen, & Gidley, 2023).In Fig. 4 (B), with the contents of SFSCP in the samples increasing, the particle size was increased. When the contents of SFSCP in sample was 4%, the particle size was the highest: D10 (7.37 nm), D50 (11.52 nm), D90 (27.38 nm), D[4.3] (18.71nm), respectively, meanwhile, when the contents of SFSCP in sample was 0%, the particle size was the lowest: D10 (4.21 nm), D50 (8.14 nm), D90 (33.67 nm), D[4.3] (13.42 nm) As shown in Fig. 2 (A) and Fig. 2 (B), as the foaming capacity, the foam stability, the gel strength and gel hardness of the samples were increased, the particle size increasing and the contents of SFSCP increasing. These particle size results were consistent with previous research findings that reported enhanced the functional properties with increasing particle size.

3.6. Secondary structure

The Raman spectral curves of different samples were shown in Fig. 5 (A). The percentage contents of secondary structures in different samples were shown in Fig. 5 (B).

Raman spectroscopy was employed as an effective analytical approach for characterizing protein secondary structures based on their distinct vibrational fingerprints (Mesias, Zhang, Fu, Dai, & Huang, 2025). The amide I band region between 1600 and 1700 cm^{-1} was specifically investigated, revealing characteristic peak positions associated with different structural motifs (Peters, Jin, Luczak, Lyons, & Kalyanaraman, 2025). a-helix were consistently observed at approximately 1650 cm^{-1}, while parallel b-sheets were detected at 1630-1640 cm^{-1} and antiparallel b-sheets at 1670-1680 cm^{-1}. Random coil conformations typically exhibited peaks at the 1660-1670 cm^{-1} range (Wang et al., 2024). Quantitative assessment of secondary structure components was achieved through mathematical deconvolution of the amide I band spectral data.

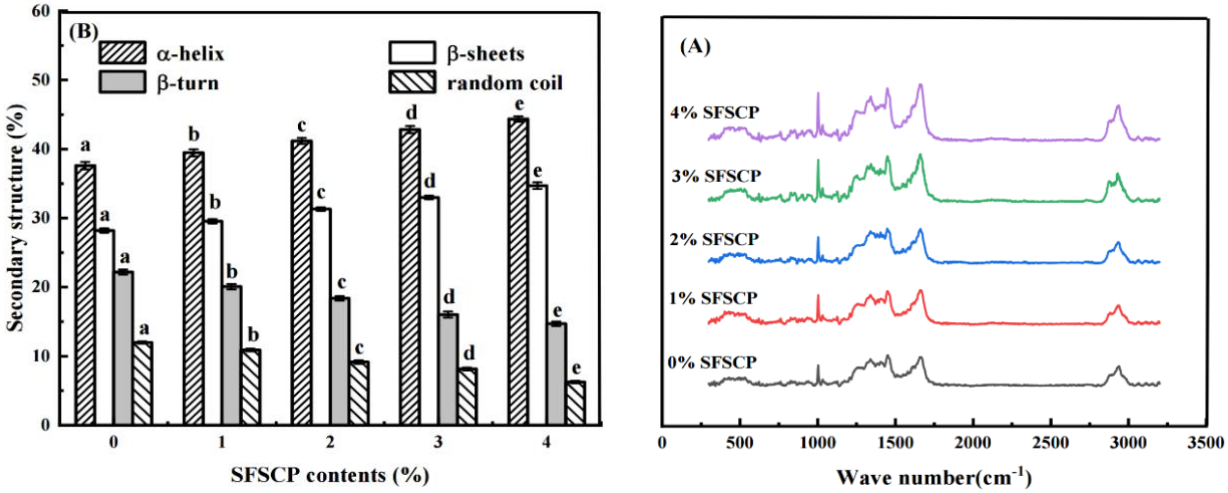

Figure 5. The secondary structure of the samples. (A) The Raman spectral curves of different samples. (B) The percentage contents of secondary structures in different samples. Three replicate samples were measured for each treatment.

With the content of SFSCP in the samples was increased, the contents of a-helix and b-sheet in the EW solution increasing, while the contents of b-turn and random coil decreasing. The content of a-helix in samples was increased from 37.61% to 44.35%, and the content of b-sheet was increased from 28.20% to 34.70%, meanwhile, the content of b-turn was decreased from 22.21% to 14.70%, and the content of random coil was decreased from 11.98% to 6.25%. The a-helix conformation was characterized by the extension of amino acid side chain R-groups toward the exterior of the helical structure. The carbonyl oxygen of each peptide bond was observed to form a fourth hydrogen bond with the N-H group, with these hydrogen bonds aligned parallel to the helix's longitudinal axis (Roessl, Leitgeb, Pieters, De Beer, & Nidetzky, 2014). In b-sheets structure all peptide bonds within the protein were found to participate in interchain hydrogen bonding. Both hydrogen bonds and van der Waals forces between adjacent peptide bonds were identified as the predominant stabilizing forces for secondary structure integrity. Random coil structures were noted to lack such well-defined hydrogen bonding patterns (Z. Yu, Liu, Zhao, Yin, Liu, & Chen, 2012). Previous studies demonstrated that the contents of a-helix and b-sheet in protein samples was positively correlated with the gel strength and hardness (Jia et al., 2026). As shown in Fig. 2 (A) and Fig. 2 (B), the foaming capacity, the foam stability, the gel strength and the gel hardness were significantly enhanced with increasing concentrations of SFSCP. These results indicated that the content of a-helix and b-sheet structures determined the gel properties of protein samples, meanwhile, adding SFSCP to EW liquid could significantly enhance the gel properties.

4. Conclusions

This study was based on proteomics and bioinformatics to investigate the amino acid sequence of peptides from SFSCP. 144 proteins were matched by using the UniProtKB database. Among them, the sequences of SFSCP were found to align with functional proteins beneficial to human health, such as calcium-transporting ATPase, apolipoproteins, and lumican, therefore, SFSCP could be considered a highly nutritious food ingredient. EW liquid is primarily used in food production with gel properties, foaming properties, improving texture, increasing volume, and enhancing stability. EW liquid was used in baked goods, confectionery, and meat products to improve taste and structure. In this study, SFSCP were added to EW, and with the contents of SFSCP increasing, the foaming and gel properties in the samples increasing, meanwhile, the contents of sulfhydryl groups, disulfide bond, a-helix, b-sheet and particle size in the samples increased, whereas the contents of b-turn, random coil and surface hydrophobicity decreased. The results demonstrated that adding SFSCP to EW liquid could enhance the nutritional value and flavor of EW products, meanwhile, could also enhance the EW functional properties.

5. References

Ali, L. A., Parhi, A., & Sharma, P. (2025). Understanding the effect of structure, composition, and particle size on the oral tribology of solid, semi-solid and liquid dairy foods. International Dairy Journal, 166, 106212.

Balis, A., Gochev, G., Truzzolillo, D., Lupa, D., Szyk-Warszynska, L., & Zawala, J. (2025). Water-in-water PEG/DEX/protein microgel emulsions: Effect of microgel particle size on the rate of emulsion phase separation. Food Hydrocolloids, 167, 111425.

Banthia, S., McKenna, A., Tiwari, S. K., & Dubey, S. P. N. (2025). DCBLSTM—Deep Convolutional Bidirectional Long Short-Term Memory neural network for Q8 secondary protein structure prediction. Computers in Biology and Medicine, 195, 110457.

Bhavsar, P. P., Kalita, B., Taunk, K., & Rapole, S. (2025). Decoding the key hallmarks of chemoresistance: A proteomic tale from breast cancer research. Biochimica et Biophysica Acta (BBA) - Reviews on Cancer, 189404.

Chi, G., Liu, H., Zu, S., Tang, B., Wang, Y., Cao, M., . . . He, N. (2024). Effects of high hydrostatic pressure treatment: Identification and characterization of snakehead-muscle-protein-based angiotensin-converting-enzyme-inhibitory peptides. LWT, 194, 115782.

De la Cruz-Torres, L. F., Rodríguez-Celestino, V., Centeno-Leija, S., Serrano-Posada, H., Ceballos-Magaña, S. G., Aguilar-Padilla, J., . . . Osuna-Castro, J. A. (2022). Development of a rapid, high-sensitivity, low-cost fluorescence method for protein surface hydrophobicity determination using a Nanodrop fluorospectrometer. Food Chemistry, 396, 133681.

Ding, L., Abou-Elsoud, M., Liu, W., Ahn, D. U., Shu, D., Cai, Z., & Huang, X. (2025). Immobilization of trypsin on resin-carriers: A novel strategy to realize controlled hydrolysis and enhance the foaming properties of pasteurized and frozen-thawed egg white. Food Chemistry, 492, 145371.

Du, C., Zhu, G., Hu, H., Duan, Z., Luo, S., Lin, L., . . . Zheng, Z. (2024). Influence of droplet size and surface hydrophobicity of soybean protein-based nanoemulsion fillers on the quality of silver carp myofibrillar protein gels. Food Chemistry: X, 24, 101866.

Geiss, O., Bianchi, I., El Hadri, H., Ponti, J., Brassinne, F., Wouters, C., . . . Barrero-Moreno, J. (2025). Particle size analysis of iron hydroxide adipate tartrate (IHAT) in a food supplement: Interlaboratory testing of a dynamic light scattering method. Journal of Food Composition and Analysis, 137, 106866.

Herman, C. E., Xu, X., Traylor, S. J., Ghose, S., Li, Z. J., & Lenhoff, A. M. (2022). Behavior of weakly adsorbing protein impurities in flow-through ion-exchange chromatography. Journal of Chromatography A, 1664, 462788.

Husted, L. B., Sørensen, E. S., & Sottrup-Jensen, L. (2003). 4-(Aminosulfonyl)-7-fluoro-2,1,3-benzoxadiazole is not specific for labeling of sulfhydryl groups in proteins as it may also react with phenolic hydroxyl groups and amino groups. Analytical Biochemistry, 314(1), 166-168.

Jia, X., Wu, Z., Jia, J., Pei, J., Ge, J., Liu, X., & Duan, X. (2026). Magnetic induction electric field: A novel physical approach to modulate egg white protein structure and interfacial properties. Food Hydrocolloids, 170, 111736.

Kim, H. D., Chang, Y. B., Suh, H. J., Han, S. H., Jang, E. Y., Sun, E. M., . . . Ahn, Y. (2025). Enhancement of skin longevity through TGF-β/Smad signaling pathway modulation by Rohu fish (Labeo rohita) collagen peptides in chronologically aged hairless mice. Food Bioscience, 63, 105841.

Kobelt, T., Lippmann, M., Wuttke, J., Wessel, H., & Zimmermann, S. (2024). Influence of ionization volume and sample gas flow rate on separation power in gas chromatography-ion mobility spectrometry. Journal of Chromatography A, 1713, 464506.

Kuo, S. F.-T., Spall, S., Emery-Corbin, S. I., Mohamed, A., Dite, T., Chow, K., . . . Webb, A. I. (2025). Quantitative Proteomic Analysis Unveils Protein Concentration Effects in Neat Urine Compared to Urine Extracellular Vesicles. Journal of Proteome Research.

Li, M., Shen, Z., Zhang, P., Peng, S., Li, X., Fang, Q., . . . Wang, G. (2025). Mitigation mechanism of α-LA on AFB1-induced hepatocyte injury in snakehead fish (Channa argus): A potential substance. Aquaculture, 603, 742425.

Li, S., Hu, G., Lin, J., Lei, Y., Liu, X., Gao, Y., . . . Li, S. (2025). Multi-coupled field processing enhanced thermal stability of egg white protein condensates through hydration effect. International Journal of Biological Macromolecules, 321, 146328.

Li, X., Sun, Z., Salama, M., Zhang, X., Shu, D., Huang, X., & Cai, Z. (2025). ATGL modulates lipid-protein interactions to restore foaming capacity in yolk-residue egg white systems. International Journal of Biological Macromolecules, 321, 146192.

Li, Y., Chang, Y., Qiu, J., Yang, L., Xue, C., & Zheng, H. (2025). Protein-templated macroporous agarose microspheres as a high-performance chromatographic medium for protein purification. Carbohydrate Polymers, 353, 123266.

Lin, Q., Sun, L., Cao, Y., Xiang, M., Guo, Y., Gao, Z., . . . Sun, W. (2025). Effect of ultrasonic treatment on the surface hydrophobicity of pyrite: Properties and mechanism of ultrasonic products. Minerals Engineering, 233, 109661.

Liu, L., Li, X., Zhang, P., Yan, W., Wu, Y., Song, H., . . . Huang, Q. (2025). Ultrasound-assisted ethanol induced gelation of egg white: Effects on gel properties, water distribution and microstructure. Ultrasonics Sonochemistry, 120, 107482.

Liu, X., Yu, Y., Liu, J., Wang, D., Li, S., Lyu, S., . . . Yang, Q. (2025). Transglutaminase-catalyzed glycosylation of egg white peptides: Structural modulation and molecular mechanism of umami enhancement via T1R1/T1R3 interactions. Food Research International, 219, 117028.

Lou, X., Lim, J., Li, B., Yu, D., & Gunaratne, J. (2025). Mass spectrometry-based proteomics pipeline for screening hazardous proteins in alternative protein-based foods. Food Chemistry, 492, 145395.

Luo, H.-L., Xu, A., & Ji, L. (2025). Rapid identification of daratumumab interference with M-protein detection using MALDI-TOF mass spectrometry: a case study involving renal light chain amyloidosis. Practical Laboratory Medicine, 46, e00493.

Ma, W., Yang, M., Wu, D., Li, Y., Wang, L.-S., El-Seedi, H. R., . . . Du, M. (2023). Fish skin gelatin-based adhesive hydrogels loading cod peptides with osteogenic activity for bone tissue engineering. Colloids and Surfaces A: Physicochemical and Engineering Aspects, 673, 131695.

Margaritis, A., Priora, R., Frosali, S., Di Giuseppe, D., Summa, D., Coppo, L., . . . Di Simplicio, P. (2011). The role of protein sulfhydryl groups and protein disulfides of

the platelet surface in aggregation processes involving thiol exchange reactions. Pharmacological Research, 63(1), 77-84.

Mesias, V. S. D., Zhang, J., Fu, W., Dai, X., & Huang, J. (2025). Enhanced characterization of protein secondary structure transitions using Raman and SERS measurements combined with 2D correlation spectroscopy and principal component analysis. Spectrochimica Acta Part A: Molecular and Biomolecular Spectroscopy, 343, 126607.

Michael, P., Panchavarnam, S., Bagthasingh, C., Palaniappan, S., Velu, R., Mohaideenpitchai, M. M., . . . David, E. P. (2024). Innate immune response of snakehead fish to Indian strain of snakehead rhabdovirus (SHRV-In) infection and the infectivity potential of the virus to other freshwater fishes. Fish & Shellfish Immunology, 149, 109577.

Ming, W., Xu, Y., Chang, H., Zhang, G., Wang, Y., & Zhang, Z. (2025). Bio-inspired designing and fabricating hydrophobic functional surface for advanced fuel cell applications: A review. Renewable and Sustainable Energy Reviews, 223, 116066.

Munawaroh, H. S. H., Pratiwi, R. N., Gumilar, G. G., Aisyah, S., Rohilah, S., Nurjanah, A., . . . Show, P.-L. (2023). Synthesis, modification and application of fish skin gelatin-based hydrogel as sustainable and versatile bioresource of antidiabetic peptide. International Journal of Biological Macromolecules, 231, 123248.

Omotosho, T. A., Danh, J. P., Abdus-Salam, A. F., Brand, K., Varghese, S. M., Siqueira, A. P. S., & Feresin, R. G. (2025). Impact of Jucara (Euterpe edulis) Supplementation on Intestinal Health of Mice Fed a High-Fat, High-Sucrose, High-Salt Diet. Current Developments in Nutrition, 9, 106633.

Peters, J., Jin, C., Luczak, A., Lyons, B., & Kalyanaraman, R. (2025). Machine learning enabled protein secondary structure characterization using drop-coating deposition Raman spectroscopy. Journal of Pharmaceutical and Biomedical Analysis, 259, 116762.

Qing, M., Zang, J., Liu, Y., Chi, Y., & Chi, Y. (2025). Glutamic acid-mediated structural reconfiguration in thermally stressed liquid egg white: Decoupling colloidal aggregation for synergistic interfacial stabilization and foamability enhancement. Food Chemistry, 492, 145318.

Rahman, Z., Zhang, Y., Tabasum, A., Yongsawatdigul, J., Huang, Q., Xiong, S., . . . Yin, T. (2025). Changes in physicochemical properties of snakehead fish slices incorporated with nano fish bones during freeze-thaw cycles: Effects of marinating methods. Food Chemistry, 474, 143215.

Roessl, U., Leitgeb, S., Pieters, S., De Beer, T., & Nidetzky, B. (2014). In Situ Protein Secondary Structure Determination in Ice: Raman Spectroscopy-Based Process Analytical Tool for Frozen Storage of Biopharmaceuticals. Journal of Pharmaceutical Sciences, 103(8), 2287-2295.

Thinthasit, A., Nugroho, D., Petsong, K., Surya, R., & Benchawattananon, R. (2025). Characterization of microbiological and physicochemical changes in traditional Thai pla ra during two-stage fermentation of snakehead fish (Channa striata). International Journal of Gastronomy and Food Science, 41, 101214.

Tseng, P.-C., Yang, W.-Y., Chen, Y.-C., Chen, Y.-P., Shiu, J.-S., & Wang, S.-Y. (2025). Optimizing the gelation, structure, and thermal stability of alkali-induced duck egg white gels with calcium chloride. Poultry Science, 104(1), 104662.

Wagner, M., Kang, J., Mercado, C., Thirumlaikumar, V. P., Gorka, M., Zillmer, H., . . . Skirycz, A. (2025). Mapping protein-metabolite interactions in E. coli by integrating chromatographic techniques and co-fractionation mass spectrometry. iScience, 28(6), 112611.

Wang, F., Cao, X., Qiu, R., Zhou, X., Wang, Y., Zhang, H., . . . Zong, X. (2024). Quantification of soluble protein content and characterization of protein secondary structure by Raman spectroscopy combined

with chemometrics. Journal of Food Composition and Analysis, 136, 106817.

Xiao, B., Hua, S., Han, S., Zhang, H., Zhang, W., Xia, N., . . . Rayan, A. M. (2025). Ultrasound-assisted covalent cross-linking of egg white protein with ferulic acid: Structure, foaming, and application in chiffon cake. Food Research International, 211, 116396.

Xu, Z., Wang, E., Wang, Y., Zhou, Y., Zeng, F., Luo, Y., . . . Hong, H. (2025). Effects of fish collagen peptides and probiotics on skin health and their potential synergistic interactions: A comprehensive review. Journal of Functional Foods, 132, 106979.

Yan, S., Han, T., Xue, H., Wang, P., Tu, Y., & Zhao, Y. (2025). The synergistic effects of NaOH and NaCl on the gel properties, digestive characteristics, and product quality of salted preserved egg white. Food Research International, 211, 116402.

Yang, F., Li, S., Zhang, X., Wang, L., & Liu, S. (2025). Single-particle collision electrochemical biosensing for DNA and protein kinase via sulfhydryl group manipulation and biomodification-free Pt nanoparticle. Sensors and Actuators B: Chemical, 426, 137099.

Yao, H., Flanagan, B. M., Williams, B. A., Mikkelsen, D., & Gidley, M. J. (2023). Particle size of dietary fibre has diverse effects on in vitro gut fermentation rate and end-products depending on food source. Food Hydrocolloids, 134, 108096.

Yao, H., Williams, B. A., Mikkelsen, D., Flanagan, B. M., & Gidley, M. J. (2023). Composition and functional profiles of human faecal microbiota fermenting plant-based food particles are related to water-holding capacity more than particle size. Food Hydrocolloids, 141, 108714.

Yu, D., Chang, X., Zeng, Q., Liu, X., Zhang, X., Liao, X., . . . Huo, J. (2025). Egg white protein-mediated modulation of yogurt gel properties: Physicochemical attributes, structural evolution, and network formation mechanisms. International Dairy Journal, 170, 106355.

Yu, Z., Liu, B., Zhao, W., Yin, Y., Liu, J., & Chen, F. (2012). Primary and secondary structure of novel ACE-inhibitory peptides from egg white protein. Food Chemistry, 133(2), 315-322.

Zhang, J., Li, M., Zhang, G., Tian, Y., Kong, F., Xiong, S., . . . Du, H. (2021). Identification of novel antioxidant peptides from snakehead (Channa argus) soup generated during gastrointestinal digestion and insights into the anti-oxidation mechanisms. Food Chemistry, 337, 127921.

Zhang, L., Qiao, Z., Liu, S., Wang, J., & Ma, C. (2024). Particle size reduction technique for NaCl crystals as effective and applicable strategy for saltiness enhancement in solid foods. LWT, 191, 115655.

Zhang, L., Zang, F., Gao, J., Chen, H., & Tong, P. (2025). Fermentation-assisted enzymatic hydrolysis improves the antioxidant activity of egg white peptides. Process Biochemistry, 157, 136-146.

Zhang, M., Hou, Y., Xia, S., Hayat, K., Hua, D., Cui, H., . . . Hussain, S. (2025). Modulating the aggregation pattern of interface myofibrillar protein in emulsion gel to enhance Na+ inhomogeneous distribution during microwave heating: The effects of hydrophobic interactions and disulfide bonding. Food Research International, 217, 116762.

Zhang, T., Gong, L., Zhang, S., Xu, H., Liu, J., & Shang, X. (2025). Enhanced thermal stability of liquid egg white via disrupting the double-network structure at the initial stage of gelation. Food Research International, 220, 117033.

Acknowledgments

I wish to acknowledge the significant contributions of my laboratory coworkers, whose expertise was instrumental to this research.